Design of a Waveguide-Coupled Nanolaser for Photonic Integration

D. Heiss,[1] V. Dolores-Calzadilla,[1] A. Fiore,[2] and M. Smit[1]

COBRA Research Institute, Eindhoven University of Technology,
Postbus 513, 5600 MB Eindhoven, The Netherlands.
[1] Photonic Integration, Department of Electrical Engineering
[2] Photonics and Semiconductor Nanophysics, Department of Applied Physics
Author e-mail address: d.heiss@tue.nl

Abstract: Semiconductor nanolasers with metallo-dielectric cavities are considered as promising light sources for ultra-dense photonic integration. We present the design of a waveguide-coupled nanolaser based on optical and electrical simulations.
OCIS codes: (130.3120) Integrated optics devices; (350.4238) Nanophotonics and photonic crystals

1. Introduction

Semiconductor nanolasers provide an attractive route towards high density photonic integrated circuits in low power applications such as optical interconnects. Such lasers exploit metallic and dielectric confinement to provide high quality factors in wavelength scale cavities with active regions well below 1μm² footprint. Additionally, the metallic confinement provides efficient cooling and cross-talk immunity between densely integrated devices. Recently, promising nanolaser designs have been demonstrated that allow room temperature operation [1,2]. For use in photonic integrated circuits it is mandatory to efficiently couple the nanolaser to a photonic waveguide. In this paper we present the design of waveguide-coupled nanolaser with a low threshold current of 120 μA and an expected output power exceeding several tens of microwatts. A schematic representation of the laser design is presented in Figure 1. The laser is compatible with a photonic platform, where a III-V membrane is bonded to a CMOS wafer using a polymer (BCB). This will enable very dense photonic circuits tightly integrated with their electrical driver and receiver circuits.

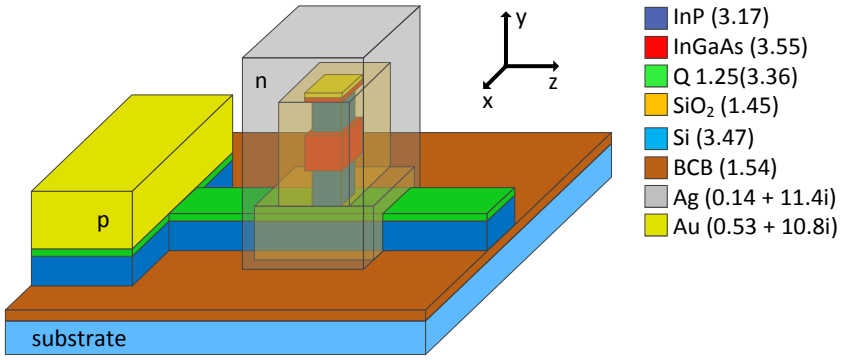

Figure 1: *Model of metallic laser coupled to an InP-membrane waveguide. The legend shows the materials and their refractive index at 1.55 μm.*

This paper is organized as follows: in section 2 we will present 3D finite-difference time-domain simulations of the cavity quality factor and coupling efficiency, which is defined as the ratio of photons leaving the cavity via the waveguide to the number of photons emitted in the active region. In section 3 we will discuss the electrical properties of the proposed layer stack calculated with the self-consistent Poisson solver and a finite element model. We will give an estimate of the threshold current, operating voltage and output power.

2. Optical simulations

The cavity dimensions were optimized using a 3D-finite-difference time-domain solver (Lumerical). A schematic of the cavity cross-section is presented in Figure 2(a), where the key parameters are highlighted. Figure 2(b) shows a typical profile of the dielectric mode considered. We optimized the quality factor and the coupling to the waveguide by changing the dielectric thickness t, the undercut s and the post height h, which is described in detail in [3]. When increasing the dielectric thickness t we find reduced optical losses in the metal cladding, while radiative leakage to

the substrate is increasing due the reduced confinement. We determined an optimal thickness t=175 nm with Silicon dioxide as the dielectric coating. The post height h is determined by a tradeoff between efficient optical coupling of the cavity to the waveguide for short post heights and a high quality factor at increased h. To limit the post height to values feasible in fabrication an undercut s is introduced, which aides decoupling the cavity from the waveguide. A good compromise between coupling efficiency and quality factor was found for h=400 nm and s=60 nm.

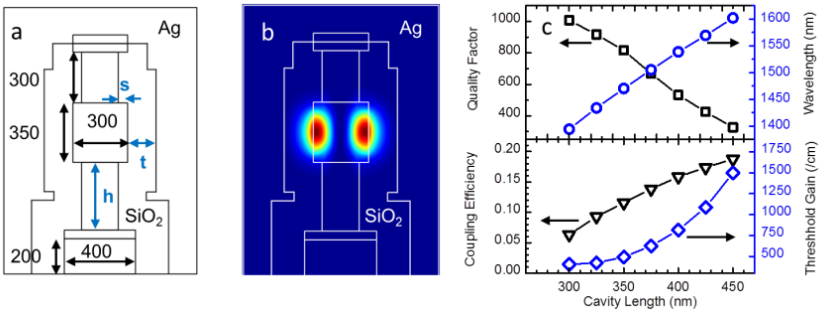

Figure 2: *(a) Schematic of the cavity cross section with dimensions indicated in nanometers. (b)Color plot of the calculated profile ($|E|^2$) of the lasing mode.(c) Quality factor (squares), resonant wavelength (circles), coupling efficiency (triangles) and the threshold material gain (diamonds) of the cavity as a function of cavity length.*

A final design parameter is the length of the cavity l, which allows adjusting the resonant wavelength of the cavity. Figure 2(c) show the quality factor (squares), resonant wavelength (circles), coupling efficiency (triangles) and the threshold material gain (diamonds) of the cavity as a function of cavity length. Other dimensions were fixed as described above. At a wavelength of 1550 nm we find a Q-factor exceeding 500 and a coupling coefficient of η=0.17. Considering the confinement factor of 0.33, as found for the mode presented in figure 2(b), this results in a material threshold gain of 750/cm for lasing operation.

3. Electrical simulations

To complement the optical simulations described above we performed electrical simulations with the self-consistent Poisson solver nextnano++ to determine the threshold current. The layer stack considered is described in table 1 and is compatible with the layout of the optical simulations.

Table 1: *Semiconductor layer stack considered for the device simulations.*

Thickness (nm)	***Material***	***Doping (/cm³)***
50	n-InGaAs	1e19
200	n-InP	5e18
100	n-InP	1e18
350	i-InGaAs	
100	p-InP	3e17
100	p-InP	5e17
100	p-InP	1e18
100	p-Q1.25	2.4e19

Carrier recombination via Auger (7e-29 cm^6/s, [4]), radiative (0.98e-10 cm^3/s,[4]) and surface recombination (5e4 cm/s, [2]) is considered in the model. We study current densities up to 200 kA/cm². In this regime surface recombination dominates the carrier dynamics. Using nextnano++ we calculated the dependence of the Fermi energies in valence and conduction band as a function of the current density in a 1-dimensional model. This allowed to calculate the optical gain with Fermi's golden rule according to reference [5] using a momentum matrix element of $2|M|^2/m_0$=25.3eV and a temperature of 300 K. The resulting gain spectra are presented in Figure 3(a) for current densities ranging from 20 to 200 kA/cm². The maximum material gain and the gain at 1550 nm is plotted in Figure 3(b) as a function of the current density. The threshold gain of 750 /cm determined by the optical simulations is reached with a current density of 100 kA/cm² corresponding to a threshold current I_{th}=120 µA for the nanolaser with an active area cross section of 300x400 nm².

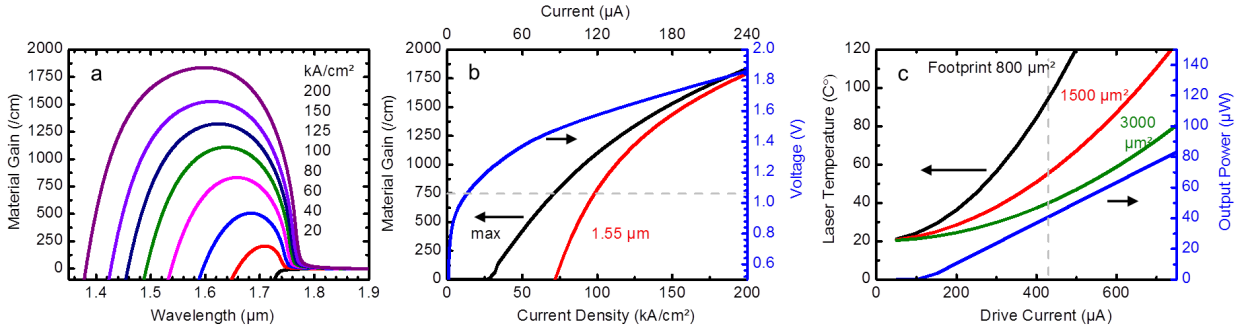

Figure 3: *(a) Material gain as a function of wavelength. (b) Material gain (left axis) and diode voltage (right axis) as a function of current density. (c) Laser temperature (left axis) and output power in the waveguide (right axis) as a function of applied current.*

We performed 3D finite element calculations (COMSOL) of the thermal and electrical properties of the device to estimate the series resistance and the achievable output power in the waveguide. We find a total series resistance of 2.25 kOhm. This is a combination of the p-side contact (400 Ohm), where the current is transported in a 100 nm thin quaternary layer on top of the waveguide, the p-doped region of the laser diode (1000 Ohm) and the ohmic contact on the n-doped side of the pillar (850 Ohm), where we assume a contact resistance of 1e-6 Ohm cm². The current-voltage characteristics of the diode including the contact resistance is plotted Figure 3(b). When driving a current through the device the high resistive regions contribute to heat generation, while the optical absorption in the metal coating of the cavity can be neglected. To calculate the laser temperature as a function of driving current we assume packaging with a high performance heat sink as described in reference [6] with a junction-to-ambient heat transfer coefficient of 7000 W/(m² K). The chip is cooled via the top-side after planarization with silicon dioxide. The metal coverage and the silicon dioxide planarization act as a heat spreading layer such that the temperature gradient across the modeled area is smaller than 5%. Therefore, the laser temperature scales roughly with the density of devices. Figure 3(c) shows the temperature in the laser as a function of the drive current calculated with the 3-dimensional finite element model for one laser per 800, 1500, and 3000 µm², respectively. The optical output power as a function of drive current I is given by $P = \eta(I - I_{th})hc/(\lambda e)$ and is plotted in Figure 3(c). Here, η=0.17 is the coupling efficiency and I_{th}=120 µA is the threshold current for an emission wavelength of λ=1.55 µm. An optical power output of 40 µW is reached for a current of 425 µA and a voltage of 1.98 V corresponding to an efficiency of 4.8%. This output power is achieved with a laser temperature of 40°C, 56°C and 95°C for the different cooling footprints, respectively. Since the heat dissipation in realistic packaging is limited, a compromise between integration density and available optical power will need to be found.

4. Conclusions

We presented the design of a metallic laser operating near 1.55 µm coupled to a thin InP waveguide. The optimized cavity has a quality factor exceeding 500 and a coupling coefficient to the waveguide of 0.17.This results in a low threshold gain of 750/cm. Electrical simulations predict a low threshold current of 120 µA. Using a high performance heat sink output powers of 40 µW seem feasible at a voltage of 1.98 V and a current of 425µA. Relaxed size constraints or more efficient cooling strategies could result in laser designs with higher output power.

This work was supported by the EU FP7 project NAVOLCHI and ERC project NOLIMITS. We would like to thank S. Birner for support with the nextnano++ software.

[1] M. T. Hill, “Status and prospects for metallic and plasmonic nano-lasers”, Journal of the Optical Society of America B, 27(11), pp. 36–44, (2010).
[2] K. Ding, M. T. Hill, Z. C. Liu, L. J. Yin, P. J. van Veldhoven, and C. Z. Ning , " Record performance of electrical injection subwavelength metallic-cavity semiconductor lasers at room temperature," Optics Express, vol. 21, p. 181703, (2013).
[3] V. Dolores-Calzadilla, D. Heiss, A. Fiore and M. Smit, "Metallo-dielectric nanolaser coupled to an InP-membrane waveguide," in *Proceedings of the 17th Annual Symposium of the IEEE Photonics Society Benelux Chapter*, (2012).
[4] C.H. Henry, R.A. Logan, F.R. Merritt, C.G. Bethea,” Radiative and nonradiative lifetimes in n-type and p-type 1.6 µm InGaAs”, Electronics Letters, 20, no.9, pp.358-359 (1984).
[5] L.A.Coldren, S.W. Corzine, and M.L.Masanovic “Gain and Current Realtions” in *Diode Lasersand Photonic Integrated Circuits”*,K. Chang, ed. (Wiley, Hoboken, NJ. 2012).
[6] Guenin, B. “Thermal Interactions Between High-Power Packages and Heat Sinks”, Electronics Cooling, Vol. 16, No. 12, (2010).